NANO LETTERS

Letter

pubs.acs.org/NanoLett

All Zinc-Blende GaAs/(Ga,Mn)As Core–Shell Nanowires with Ferromagnetic Ordering

Xuezhe Yu,[†] Hailong Wang,[†] Dong Pan,[†] Jianhua Zhao,*[,†] Jennifer Misuraca,[‡] Stephan von Molnár,[‡] and Peng Xiong[‡]

[†]State Key Laboratory of Superlattices and Microstructrues, Institute of Semiconductors, Chinese Academy of Sciences, P.O. Box 912, Beijing 100083, China

[‡]Department of Physics, Florida State University, Tallahassee, Florida 32306, United States

Supporting Information

ABSTRACT: Combining self-catalyzed vapor–liquid–solid growth of GaAs nanowires and low-temperature molecular-beam epitaxy of (Ga,Mn)As, we successfully synthesized all zinc-blende (ZB) GaAs/(Ga,Mn)As core–shell nanowires on Si(111) substrates. The ZB GaAs nanowire cores are first fabricated at high temperature by utilizing the Ga droplets as the catalyst and controlling the triple phase line nucleation, then the (Ga,Mn)As shells are epitaxially grown on the side facets of the GaAs core at low temperature. The growth window for the pure phase GaAs/(Ga,Mn)As core–shell nanowires is found to be very narrow. Both high-resolution transmission electron microscopy and scanning electron microscopy observations confirm that all-ZB GaAs/(Ga,Mn)As core–shell nanowires with smooth side surface are obtained when the Mn concentration is not more than 2% and the growth temperature is 245 °C or below. Magnetic measurements with different applied field directions provide strong evidence for ferromagnetic ordering in the all-ZB GaAs/(Ga,Mn)As nanowires. The hybrid nanowires offer an attractive platform to explore spin transport and device concepts in fully epitaxial all-semiconductor nanospintronic structures.

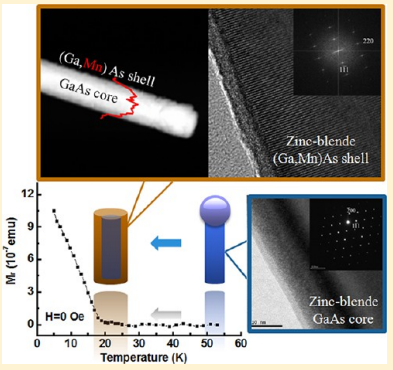

KEYWORDS: *Magnetic semiconductors, zinc-blende nanowire, magnetic property, molecular-beam epitaxy*

Diluted magnetic semiconductors (DMSs), which possess characteristics of both semiconductors and ferromagnets, are a class of magnetic materials that have garnered significant interest in the past two decades. Among them, transition metal doped III–V semiconductors, best exemplified by (Ga,Mn)As,[1,2] are studied most extensively because of the large magnetization and relatively high Curie temperature (T_c). These materials have not only yielded rich spin-dependent physics but also engendered the discoveries of many novel spintronic functionalities, such as tunneling anisotropic magnetoresistance[3] and electric field-controlled ferromagnetism,[4,5] which have been successfully incorporated into metal-based spintronics.[6−11] In a separate line of research, bottom-up synthesis and physical characterizations of semiconductor nanowires (NWs), including those of III–Vs, have been widely explored. The primary objectives are to produce nanoscale building blocks for various functional semiconductor devices[12,13] as well as to investigate the emergence of novel phenomena under extreme spatial confinement. There is natural interest in combining these two classes of materials, namely, in producing DMS NWs that exhibit robust ferromagnetism and perhaps even offer an alternative route for enhancing the magnetic properties of the DMS.[14,15] An intriguing example is the observation by us that the Curie temperature of top-down fabricated (Ga,Mn)As nanostructures could be improved to 200 K,[16] beyond the highest value attainable in the (Ga,Mn)As films.[17] It is conceivable that (Ga,Mn)As NWs fabricated from bottom-up self-assembly and absent of any surface damage from lithographic patterning would be more conducive to the optimization of the magnetic properties.

In recent years, the fabrication of self-assembled (Ga,Mn)As NWs have been reported by several groups.[18−24] In the case of pure (Ga,Mn)As, the temperatures required for NW growth were found to be higher than those yielding single-phase (Ga,Mn)As in thin film growth, raising questions regarding the phase purity of the resulting (Ga,Mn)As NWs.[1,2] Both the Mn-induced[18] or MnAs island-induced[19] growth mechanisms and the reported observations of room-temperature ferromagnetism[20,21] reinforced such skepticism. The latter has frequently resulted from MnGa or MnAs clustering. To overcome this problem, a core–shell approach was employed:[22,23] a single-crystalline GaAs core is synthesized under regular vapor–liquid–solid (VLS) growth conditions and then a (Ga,Mn)As shell is grown on the side facets of the core using low-temperature molecular-beam epitaxy (MBE) to prevent phase segregation. An alternative pathway involves ion implantation

Received: December 23, 2012
Revised: March 5, 2013
Published: March 21, 2013

of Mn into VLS-grown GaAs NWs.[24] In all these cases, however, the VLS growth of the GaAs (core) NWs utilized Au nanoparticles as the catalyst. It is well-known that GaAs NWs grown by such a method usually have the wurtzite (WZ) crystal structure or zinc-blende (ZB)/wurtzite polytypism as a result of triple phase line nucleation.[25,26] This is of great importance because (Ga,Mn)As films are acknowledged to exhibit robust ferromagnetism when they are grown epitaxially in ZB structure on ZB-GaAs substrates.[27] Actually, all of our knowledge on (Ga,Mn)As has almost been from ZB structure (Ga,Mn)As films. The consistency of crystalline phase is desirable when the system put into the test bed to explore the physics of (Ga,Mn)As in nanosize.

In contrast, self-catalyzed VLS growth via Ga nanodroplets favors the ZB structure owing to a much lower surface energy of liquid Ga than that of Au−Ga alloys, which makes triple phase line nucleation energetically unfavorable and eventually suppresses the WZ phase.[28−30] This mechanism makes it possible to control the crystal structure of the resulting GaAs NWs, enabling the synthesis of NWs with pure-ZB body and even heterohomo-superlattices as demonstrated in our recent work.[31] The GaAs NWs with pure zinc-blende structure along the whole length are clearly the more preferable choice than the NWs with ZB/WZ polytypism or WZ structure as the "core" for the growth of the (Ga,Mn)As shell with optimal magnetic properties.

In this Letter, we report successful fabrication of all-ZB GaAs/(Ga,Mn)As core−shell nanowires on Si(111) substrates by MBE. The process is consisted first of self-catalyzed VLS growth of pure-ZB GaAs core naowires (with the exception of a very short WZ section at the tip[31]), followed by low-temperature MBE growth of the (Ga,Mn)As shells on the side facets of the GaAs cores. We find the growth window for pure phase GaAs/(Ga,Mn)As core−shell NWs to be very narrow. The all-ZB GaAs/(Ga,Mn)As core−shell structure is obtained when Mn concentration is not more than 2% and growth temperature is 245 °C or below. The core−shell morphologies and crystal structures are confirmed by the high-resolution transmission electron microscopy and scanning electron microscopy. Magnetic measurements with SQUID confirm the ferromagnetic ordering in the GaAs/(Ga,Mn)As core−shell nanowires.

The samples were grown in a V80 MARKI MBE system. Commercial n-type Si (111) wafers were used as the substrates. The pretreatment of the substrates was described in the ref 31.The growth of GaAs core NWs was performed at 640 °C with the V/III ratio fixed at 3:1. An As flux of 6×10^{-6} mbar was used. The (Ga,Mn)As shell deposition followed GaAs NW growth. We employed the low-temperature MBE technique at the typical growth conditions for pure-phase (Ga,Mn)As films.[1] As_4 pressure was increased while the Ga cell temperature was kept constant in order to obtain a V/III ratio of 15 for the shell growth. The deposited (Ga,Mn)As has a nominal film-equivalent thickness of 300 nm. Several combinations of different Mn concentrations and substrate temperatures (T_s) were attempted to identify the optimal growth parameters.

Figure 1 shows a series of scanning electron microscopy (SEM) images of a typical GaAs core growth. The NWs were grown vertically on a substrate to a length of about 3 μm, a uniform diameter of 90 nm, and a surface density of around 7/μm^2 (Figure 1a,b). While most NWs show the obvious shape of a Ga droplet at the tip (Figure 1a,b), indicative of the VLS growth mechanism, some had lost the Ga droplets due to the

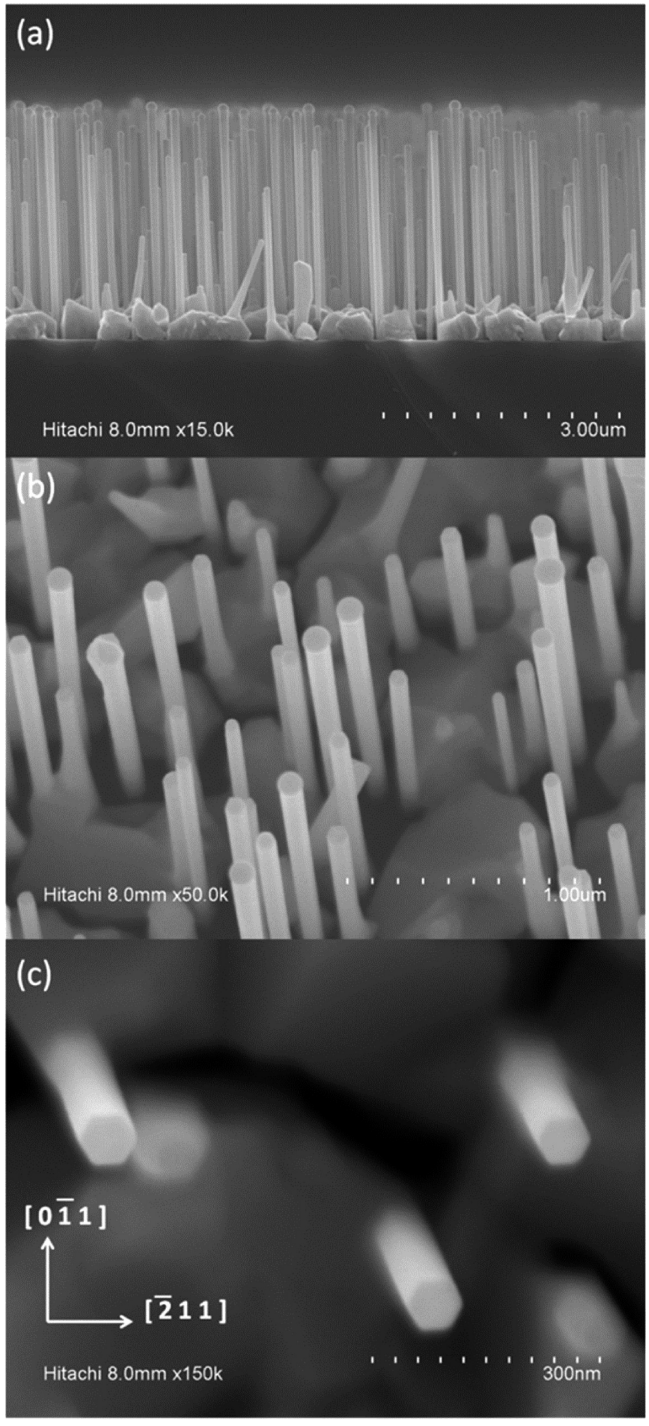

Figure 1. Scanning electron microscopy images of self-catalyzed GaAs NWs grown on Si(111). (a) Side view, and (b) top view inclined at 15°, for an assembly of as-grown NWs. (c) High-magnification SEM image, confirming the side facets as {1$\bar{1}$0} surfaces.

crystallization in ambient arsenic during the cool down.[31] By studying the top view images of the NWs, we observed that the NW side surface is consisted of six facets, which is common for III−V NWs grown on (111) oriented substrates.[32] Furthermore, the SEM measurement identified the six facets as belonging to the {0$\bar{1}$1} surface family (Figure 1c). While many groups have reported self-catalyzed growth of GaAs NWs with pure ZB structure,[30,31,33] we note that WZ structure GaAs NWs can result from the same approach, especially when a relatively

dx.doi.org/10.1021/nl304740k | Nano Lett. 2013, 13, 1572−1577

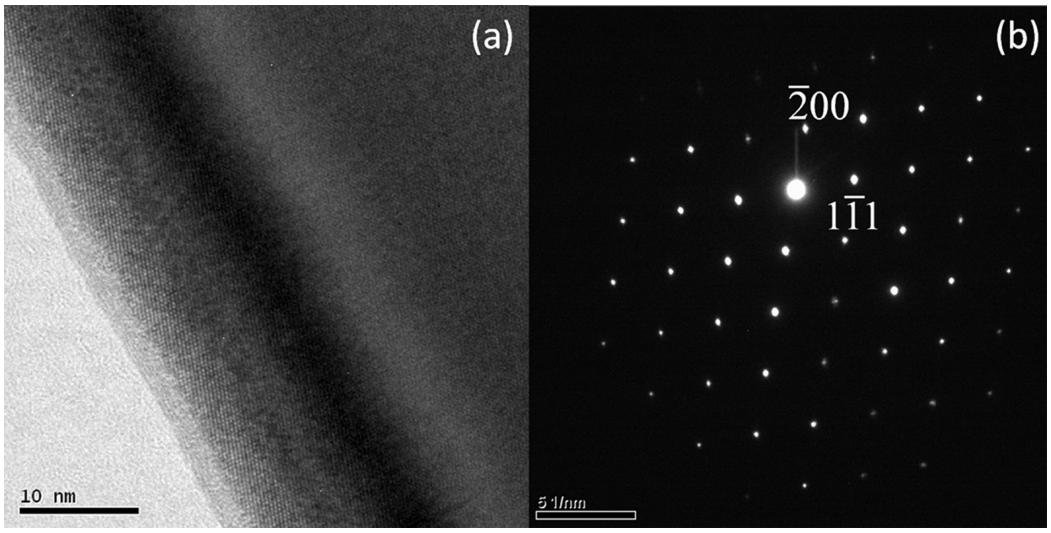

Figure 2. (a) HRTEM and (b) SAD images of an as-grown GaAs NW. The electron beam was aligned along the $[1\bar{1}0]$ direction.

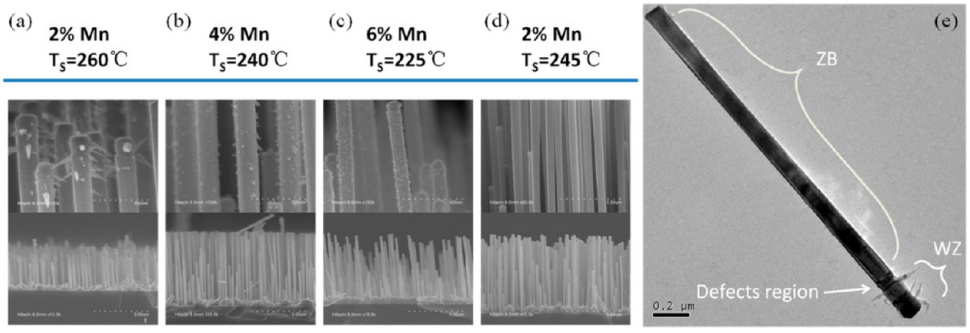

Figure 3. (a–d) SEM images of the final GaAs/(Ga,Mn)As NWs with different growth conditions for (Ga,Mn)As. From left to right: (a) branched growth only near the apex on the side facets of the GaAs core, (b) branched growth on the side facets on the entire NW, (c) nanocrystal growth on the NW surfaces, (d) smooth growth on the side facets of the GaAs core. (e) TEM image of a GaAs/(Ga,Mn)As core–shell NW grown under conditions in (a) (2% Mn at 260 °C). The NW has a ZB bulk and WZ tip separated by a distinct defect section.

low As beam flux is used.[33,34] In addition, our recent investigation shows that a low growth temperature leads to significant number of twin plane defects in the NWs. Our choices of large arsenic flux and high growth temperature are amenable to producing GaAs NWs in pure ZB structure with minimal twin plane defects, as shown in Figure 2a,b. It is shown that by controlling the triple phase line nucleation, pure ZB structure is obtained along the length of the GaAs NWs, with the exception of a very short WZ section (~100 nm) at the tip (Supporting Information).

MBE growth of (Ga,Mn)As shells were performed on the as-prepared GaAs NWs, followed by a systematic examination of the morphology (Figure 3a–d). Having tried various growth conditions, it is found that the growth window for the successful fabrication of the (Ga,Mn)As shell, that is, uniform and smooth growth on the NW side facets, is much more limited than that for two-dimensional (Ga,Mn)As films. Among these samples, GaAs/(Ga,Mn)As core–shell NWs with perfect side facets were obtained at T_s of 245 °C or lower at 2% Mn content. Unsuccessful attempts, in the forms of branched growth or nanocrystals on the sidewalls, are most likely due to the non-(001) side facets of the GaAs core, which presents a different growth condition than the usual GaAs (001) surfaces. For large Mn content and low T_s, nanocrystals appear on the sidewalls, which may have originated from Mn aggregation in the nonuniform deposition of the shell layer on the vertical GaAs NW cores and the limited diffusion distance for the Mn at the low T_s. On the other hand, the branched growths are probably GaAs NWs catalyzed by MnAs nanoislands.[19] An interesting observation is made from the sample with 2% Mn concentration grown at 260 °C. The SEM image in Figure 3a reveals that the nanobranches appear mainly near the apex, while the rest of the sidewalls was mostly smooth. Recalling the observation in our recent work[31] (also see Supporting Information), it is evident that the nanobranch growth occurs only on the short WZ section. The conclusion is confirmed directly by a transmission electron microscopy (TEM) measurement on one NW (Figure 3e). The ZB length and WZ tip of the NW is separated by a distinct region with high density of twin-plane and stacking fault defects, and the nanobranches are present only on the WZ section. This clearly relates to the differences in the MnAs formation conditions on facets of the different crystal structures. On the basis of the SEM measurements on the NWs before and after the (Ga,Mn)As shell deposition, we observed that these shells have an average thickness of 30–40 nm, much less than the nominal thickness of the (Ga,Mn)As film, which is, nonetheless, qualitatively expected due to the orientation and high aspect ratio of the NWs.

More detailed TEM measurements were implemented on GaAs/(Ga,Mn)As core–shell NWs exhibiting smooth shell growth. A typical image and the corresponding selected area

dx.doi.org/10.1021/nl304740k | *Nano Lett.* 2013, 13, 1572–1577

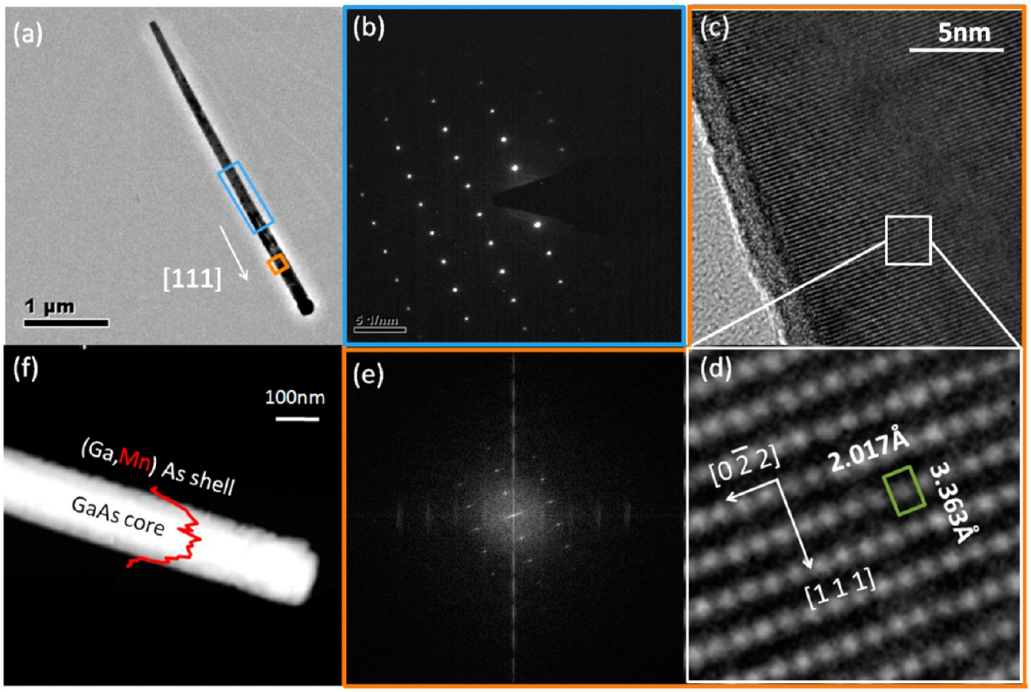

Figure 4. TEM images for GaAs/(Ga,Mn)As (2% Mn) core−shell NWs grown at 245 °C. (a) A single core−shell nanowire. (b) SAD pattern taken from the section of the NW indicated by the blue rectangle in (a), showing zinc-blende structure with the electron beam aligned along the $[\bar{2}11]$ direction. (c) HRTEM image near the side facet (inside the orange box in (a)). (d) Further magnified image for a region in (c), with the corresponding FFT (e) of the HRTEM image. (f) Energy dispersive X-ray spectroscopy line profile along the diameter direction for Mn in a single GaAs/(Ga,Mn)As NW.

diffraction (SAD) are presented in Figure 4a,b. The results confirm the pure ZB structure. Dissimilar to the highly mismatched GaAs/InAs core−shell NWs, for which there was a splitting of the spot in the SAD pattern,[35] a unique pattern is observed in the SAD particularly, indicating the same crystal structure for the (Ga,Mn)As shell and the GaAs core and epitaxial growth of the (Ga,Mn)As shell on the side facets of the GaAs core. The fast Fourier transform (FFT) of an high-resolution transmission electron mcroscopy (HRTEM) image near the sidewall (Figure 4e) is consistent with the SAD pattern, providing further support for our conclusion. Because of the low Mn concentration (~2%), no distinct boundary between the (Ga,Mn)As shell region and the GaAs NW region is evident in the TEM images. However, as shown in Figure 4c,d, HRTEM performed near the sidewall of the NW (indicated by the orange box in Figure 4) yielded a much larger averge lattice spacing of 3.36 Å between the neighboring (111) planes, in contrast to 3.264 Å for bulk GaAs and 3.273 Å for pure-ZB GaAs NWs. Although Mn impurities and As antisite defects are known to induce increase of the lattice constants in (Ga,Mn)As,[27] the observed large increase of the lattice spacing in the [111] direction, in the deposition plane instead of growth direction, cannot be explained in the same manner. We attribute this to low-temperature growth of shell layer on the nonpolar $(0\bar{1}1)$ surface, which introduces structural defects. Along the (Ga,Mn)As shell growth direction $[0\bar{1}1]$, the lattice constant is 2.017 Å, a little larger than the bulk value of 1.998 Å. Figure 4f shows the energy dispersive X-ray spectroscopy (EDX) line profile scanned along the diameter of the NW, which offers a confirmation of the Mn doping in the shell. In (Ga,Mn)As films, it is well-known that Mn can occupy Ga sites (Mn_{Ga}),[36] as well as the two interstitial sites surrounded by four Ga or As atoms (Mn_I).[37] At temperatures lower than T_s, Mn_{Ga} are energetically favorable and considered to be stable, while Mn_I are rather mobile and can be partly eliminated from the GaAs matrix by low-temperature thermal annealing.[38] Our samples have a nominal total Mn content of 2%, a level much below the concentration at which Mn_I become significant.[37] Therefore, in these core−shell NWs most of the Mn dopants are expected to be Mn_{Ga} and well confined in the shell layer.

During NWs growth, a polycrystalline GaAs layer results from growth on the silicon-dioxide surface (Figure 1b).[39] The subsequent (Ga,Mn)As deposition may produce polycrystalline Mn−Ga−As alloy clusters, which could contribute to the overall magnetic signal of measurements on ensembles of GaAs/(Ga,Mn)As NWs. The magnetic response from these substance could skew or even mask that from the NWs.[40] Such contributions in our samples, however, are expected to be isotropic with respect to the applied magnetic field, while the magnetization of the (Ga,Mn)As shells of the NWs should exhibit strong anisotropy. Our magnetic measurements indeed show unusual magnetic behavior indicative of a superposition of isotropic and anisotropic contributions. The inset of Figure 5a shows the overall $M-H$ behavior at 5 K for a sample of an ensemble of GaAs/(Ga,Mn)As NWs on a Si substrate, with the applied magnetic field parallel (black, [111] direction) and perpendicular (red, $[1\bar{1}0]$ direction) to the length of the NWs, which exhibit little difference between the high-field behaviors for the two field directions. This is in contrast to the results of similar measurements on (Ga,Mn)As films.[41] It has been shown in a number of DMSs that spinodal decomposition leads to chemical phase separation in the film matrix. Although spinodal decomposition can occur in the high-temperature annealed (Ga,Mn)As[42,43] and polycrystalline films such as the material on the SiO_2 substrate in this work, as-grown and low-

dx.doi.org/10.1021/nl304740k | Nano Lett. 2013, 13, 1572−1577

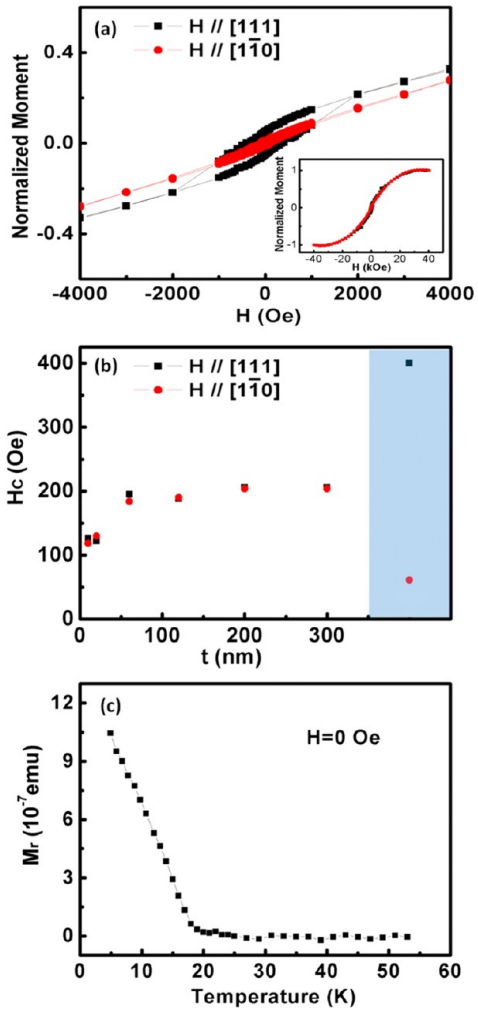

Figure 5. (a) Magnetic hysteresis loops at 5 K for a sample of GaAs/(Ga,Mn)As core−shell NWs on Si(111) substrate with the (Ga,Mn)As grown under optimal conditions (2% Mn at 245 °C). Black squares (red circles) are for field applied parallel (perpendicular) to the length of the NWs. The inset shows a large $M-H$ scan. (b) The coercive field parallel (red circles) and perpendicular (black squares) to the substrate surface for a series of reference samples at increasing nominal thicknesses of (Ga,Mn)As. The (Ga,Mn)As is deposited under the same conditions as in (a) but on Si substrates fully covered with SiO_2. The coercive fields for the GaAs/(Ga,Mn)As core−shell NWs are presented (blue region) for direct comparison. (c) The temperature dependence of the remnant magnetization of the GaAs/(Ga,Mn)As core−shell NWs measured with increasing temperature from 5 K and no applied field.

temperature annealed epitaxial (Ga,Mn)As exhibits uniform intrinsic ferromagnetism attributed to the ferromagnetic interaction between Mn_{Ga}.[2] In our core−shell NWs, TEM measurements have provided clear evidence for the epitaxy of the as-grown (Ga,Mn)As shells and produced no indication of phase separation or formation of nanoparticles. Contrary to the high-field region, in the low-field part, the magnetic hysteresis show marked differences between the two field directions (Figure 5a), which we attribute to the predominance of the magnetization from the (Ga,Mn)As shells at low field, manifested by the anisotropy of the magnetic NWs. Such effects of anisotropy are shown to contribute significantly to the magnetization in DMS NWs, especially in Mn-doped III−V semiconductor NWs.[22,44] To unambiguously demonstrate the ferromagnetism of the GaAs/(Ga,Mn)As core−shell NWs, we fabricated a series of samples with different nominal thicknesses, which is up to 300 nm, of (Ga,Mn)As, following exactly the same procedure for the growth of the GaAs/(Ga,Mn)As core−shell NWs described above. For this series of samples, however, we used Si(111) substrates completely covered by silicon-dioxide. As a consequence, no NWs were grown but one expects the same polycrystalline and/or granular materials on the substrates. Figure 5b shows the out-of-plane (black) and in-plane (red) coercive fields for this series of samples. For comparison, the coercive fields parallel and perpendicular to the length of the NWs for the sample with GaAs/(Ga,Mn)As core−shell NWs are given on the same plot (blue region). Evidently, all of the reference samples exhibit essentially the same coercive field for both field orientations, while for the core−shell NWs, the coercive field along the NW axis direction is much larger than that perpendicular to it. This result convincingly demonstrates that the low-field magnetization with the applied field parallel to the NW length shown in Figure 5a predominantly reflects the ferromagnetic response of the GaAs/(Ga,Mn)As core−shell NWs. In particular, the remnant magnetization in this field orientation is almost solely due to the NWs. Having established this, we then performed measurement of the temperature dependence of the magnetization of the GaAs/(Ga,Mn)As NWs: The sample was cooled down to 5 K in zero field and then magnetized along the length of the NWs, the remnant moment of the sample was measured while being heated up with no applied field. Figure 5c shows the result of the measurement. Within the temperature range of the measurement, a single transition temperature T_c of 18 K was found, which is, based on the above considerations, attributed to the ferromagnetic ordering of the GaAs/(Ga,Mn)As NWs. So far, besides the most commonly used GaAs(001), (Ga,Mn)As films have been synthesized on GaAs substrates of several different orientations including (110), (311), (411)A, all of which have exhibited robust ferromagnetism.[45−48] However, the highest T_c's for (Ga,Mn)As are always achieved in those grown on the GaAs (001) substrates.[17,48] Wilson et al.[48] attributed the lower T_c in films of other orientations to the dependence of the formation of As antisites (which leads to the increase of compensation effect), rather than the efficiency of Mn incorporation, on the orientation of the growth surface. The combination of the low Mn concentration and the non-(001) side facets of GaAs NW cores likely result in the relatively low T_c of the (Ga,Mn)As shells.

In conclusion, single phase all-ZB GaAs/(Ga,Mn)As core−shell NWs have been synthesized via self-catalyzed VLS growth of the GaAs core and low-temperature MBE deposition of (Ga,Mn)As. In spite of the magnetic background, robust ferromagnetism in the GaAs/(Ga,Mn)As core−shell NWs has been established beyond ambiguity. The hybrid system of a conventional semiconductor core and DMS shell provides an intrinsic nanoscale platform to examine spin-dependent physics and explore new device concepts in all-semiconductor spintronics.

■ ASSOCIATED CONTENT

Ⓢ Supporting Information

Additional information and figures. This material is available free of charge via the Internet at http://pubs.acs.org.

dx.doi.org/10.1021/nl304740k | *Nano Lett.* 2013, 13, 1572−1577

AUTHOR INFORMATION

Corresponding Author

*E-mail: jhzhao@red.semi.ac.cn.

Notes

The authors declare no competing financial interest.

ACKNOWLEDGMENTS

J.H.Z. thanks MOST of China for Grant 2012CB932701 and NSFC for Grants 60836002 and 10920101071. S.v.M. and P.X. acknowledge NSF Materials World Network Grant DMR-0908625.

REFERENCES

(1) Ohno, H.; Shen, A.; Matsukura, F.; Oiwa, A.; Endo, A.; Katsumoto, S.; Iye, Y. *Appl. Phys. Lett.* **1996**, *69*, 363.

(2) Ohno, H. *Science* **1998**, *281*, 951.

(3) Gould, C.; Rüster, C.; Jungwirth, T.; Girgis, E.; Schott, G. M.; Giraud, R.; Brunner, K.; Schmidt, G.; Molenkamp, L. W. *Phys. Rev. Lett.* **2004**, *93*, 11.

(4) Ohno, H.; Chiba, D.; Matsukura, F.; Omiya, T.; Abe, E.; Dietl, T.; Ohno, Y.; Ohtani, K. *Nature* **2000**, *408*, 944.

(5) Chiba, D.; Yamanouchi, M.; Matsukura, F.; Ohno, H. *Science* **2003**, *301*, 943.

(6) Sinova, J.; Žutić, I. *Nat. Mater.* **2012**, *11*, 368.

(7) Gao, L.; Jiang, X.; Yang, S. H.; Burton, J. D.; Tsymbal, E. Y.; Parkin, S. S. P. *Phys. Rev. Lett.* **2007**, *99*, 226602.

(8) Park, B. G.; Wunderlich, J.; Martí, X.; Holý, V.; Kurosaki, Y.; Yamada, M.; Yamamoto, H.; Nishide, A.; Hayakawa, J.; Takahashi, H.; Shick, A. B.; Jungwirth, T. *Nat. Mater.* **2011**, *10*, 347.

(9) Ohno, H. *Nat. Mater.* **2010**, *9*, 952.

(10) Yamada, Y.; Ueno, K.; Fukumura, T.; Yuan, H. T.; Shimotani, H.; Iwasa, Y.; Gu, L.; Tsukimoto, S.; Ikuhara, Y.; Kawasaki, M. *Science* **2011**, *332*, 1065.

(11) Chiba, D.; Fukami, S.; Shimamura, K.; Ishiwat, N.; Kobayashi, K.; Ono, T. *Nat. Mater.* **2011**, *10*, 853.

(12) Lu, W.; Lieber, C. M. *Nat. Mater.* **2007**, *6*, 841.

(13) Li, Y.; Qian, F.; Xiang, J.; Lieber, C. M. *Mater. Today* **2006**, *9*, 18.

(14) Choi, H. J.; Seong, H. K.; Chang, J. Y.; Lee, K. I.; Park, Y. J.; Kim, J. J.; Lee, S. K.; He, R. R.; Kuykendall, T.; Yang, P. D. *Adv. Mater.* **2005**, *17*, 1351.

(15) Radovanovic, P. V.; Barrelet, C. J.; Gradečak, S.; Qian, F.; Lieber, C. M. *Nano Lett.* **2005**, *5*, 1407.

(16) Chen, L.; Yang, X.; Yang, F. H.; Zhao, J. H.; Misuraca, J.; Xiong, P.; von Molnár, S. *Nano Lett.* **2011**, *11*, 2584.

(17) Chen, L.; Yan, S.; Xu, P. F.; Lu, J.; Wang, W. Z.; Deng, J. J.; Qian, X.; Ji, Y.; Zhao, J. H. *Appl. Phys. Lett.* **2009**, *95*, 182505.

(18) Martelli, F.; Rubini, S.; Piccin, M.; Bais, G.; Jabeen, F.; Franceschi, S. D.; Grillo, V.; Carlino, E.; D'Acapito, F.; Boscherini, F.; Cabrini, S.; Lazzarino, M.; Businaro, L.; Romanato, F.; Franciosi, A. *Nano Lett.* **2006**, *6*, 2130.

(19) Sadowski, J.; Dluzewski, P.; Kret, S.; Janik, E.; Lusakowska, E.; Kanski, J.; Presz, A.; Terki, F.; Charar, S.; Tang, D. *Nano Lett.* **2007**, *7*, 2724.

(20) Kim, H. S.; Cho, Y. J.; Kon, K. J.; Kim, C. H.; Chung, G. B.; Park, J. H.; Kim, J. Y.; Yoon, J. B.; Jung, M. H.; Jo, Y. H.; Kim, B. S.; Ahn, J. P. *Chem. Mater.* **2009**, *21*, 1137.

(21) Jeon, H. C.; Kang, T. W.; Kim, T. W.; Yu, Y. J.; Jhe, W.; Song, S. A. *J. Appl. Phys.* **2007**, *101*, 023508.

(22) Rudolph, A.; Soda, M.; Kiessling, M.; Wojtowicz, T.; Schuh, D.; Wegscheider, W.; Zweck, J.; Back, C.; Reiger, E. *Nano Lett.* **2009**, *9*, 3860.

(23) Butschkow, C. H.; Reiger, E.; Geißler, S.; Rudolph, A.; Soda, M.; Schuh, D.; Woltersdorf, G.; Wegscheider, W.; Weiss, D. cond-mat arXiv:1110.5507v1.

(24) Borschel, C.; Messing, M. E.; Borgström, M. T.; Paschoral, W., Jr.; Wallentin, J.; Kumar, S.; Mergenthaler, K.; Deppert, K.; Canali, C. M.; Pettersson, H.; Samuelson, L.; Ronning, C. *Nano Lett.* **2011**, *11*, 3935.

(25) Glas, F.; Harmand, J. C.; Patriarche, G. *Phy. Rev. Lett.* **2007**, *99*, 146101.

(26) Dick, K. A.; Caroff, P.; Bolinsson, J.; Messing, M. E.; Johansson, J.; Deppert, K.; Wallenberg, L. R.; Samuelson, L. *Semicond. Sci. Technol.* **2010**, *25*, 024009.

(27) Jungwirth, T.; Sinova, J.; Mašek, J.; Kučera, J.; MacDonald, A. H. *Rev. Mod. Phys.* **2006**, *78*, 809.

(28) Cirlin, G. E.; Dubrovskii, V. G.; Samsonenko, Y. B.; Bouravleuv, A. D.; Durose, K.; Proskurvakov, Y. Y.; Mendes, B.; Bowen, L.; Kaliteevski, M. A.; Abram, R. A.; Zeze, D. *Phys. Rev. B* **2010**, *82*, 035302.

(29) Krogstrup, P.; Curiotto, S.; Johnson, E.; Aagesen, M.; Nygård, J.; Chatain, D. *Phy. Rev. Lett.* **2011**, *106*, 125505.

(30) Dubrovskii, V. G.; Cirlin, G. E.; Sibirev, N. V.; Jabeen, F.; Harmand, J. C.; Werner, P. *Nano Lett.* **2011**, *11*, 1247.

(31) Yu, X. Z.; Wang, H. L.; Lu, J.; Zhao, J. H.; Misuraca, J.; Xiong, P.; von Molnár, S. *Nano Lett.* **2012**, *12*, 5436.

(32) Fortuna, S. A.; Li, X. L. *Semicond. Sci. Technol.* **2010**, *25*, 024005.

(33) Spirkoska, D.; Arbiol, J.; Gustafsson, A.; Conesa-Boj, S.; Glas, F.; Zardo, I.; Heigoldt, M.; Gass, M. H.; Bleloch, A. L.; Estrade, S.; Kaniber, M.; Rossler, J.; Peiro, F.; Morante, J. R.; Abstreiter, G.; Samuelson, L.; Fontcuberta i Morral, A. *Phys. Rev. B* **2009**, *80*, 245325.

(34) Yamaguchi, M.; Paek, J. H.; Amano, H. *Nanoscale Res. Lett.* **2012**, *7*, 558.

(35) Popovitz-Biro, R.; Kretinin, A.; Von Huth, P.; Shtrikman, H. *Cryst. Growth Des.* **2011**, *11*, 3858.

(36) Shioda, R.; Ando, K.; Hayashi, T.; Tanaka, M. *Phys. Rev. B* **1998**, *58*, 1100.

(37) Yu, K. M.; Walukiewicz, W.; Wojtowicz, T.; Kuryliszyn, I.; Liu, X.; Sasaki, Y.; Furdyna, J. K. *Phys. Rev. B* **2002**, *65*, 201303(R).

(38) Edmonds, K. W.; Boguslawski, P.; Wang, K. Y.; Campion, R. P.; Novikov, S. N.; Farley, N. R. S.; Gallagher, B. L.; Foxon, C. T.; Sawicki, M.; Dietl, T.; Nardelli, M. B.; Bernholc, J. *Phys. Rev. Lett.* **2004**, *92*, 3.

(39) Hong, J. M.; Wang, S.; Sands, T.; Washburn, J.; Flood, J. D.; Merz, J. L.; Low, T. *Appl. Phys. Lett.* **1986**, *48*, 142.

(40) Cooley, B. J.; Clark, T. E.; Liu, B. Z.; Eichfeld, C. M.; Dickey, E. C.; Mohney, S. E.; Crooker, S. A.; Samarth, N. *Nano Lett.* **2009**, *9*, 3142.

(41) Liu, X.; Furdyna, J. K. *J. Phys.: Condens. Matter* **2006**, *18*, 245.

(42) Yokoyama, M.; Yamaguchi, H.; Ogawa, T.; Tanaka, M. *J. Appl. Phys.* **2005**, *97*, 10D317.

(43) Moreno, M.; Jenichen, B.; Kaganer, V.; Braun, W.; Trampert, A.; Däweritz, L.; Ploog, K. H. *Phys. Rev. B* **2003**, *67*, 235206.

(44) Hegde, M.; Farvid, S. S.; Hosein, I. D.; Radovanovic, P. V. *ACS Nano* **2011**, *5*, 6365.

(45) Wurstbauer, U.; Sperl, M.; Soda, M.; Neumaier, D.; Schuh, D.; Bayreuther, G.; Zweck, J.; Wegscheider, W. *Appl. Phys. Lett.* **2008**, *92*, 102506.

(46) Wang, K. Y.; Edmonds, W.; Zhao, L. X.; Sawicki, M.; Campion, R. P.; Gallagher, B. L.; Foxon, C. T. *Phys. Rev. B* **2005**, *72*, 115207.

(47) Omiya, T.; Matsukura, F.; Shen, A.; Ohno, Y.; Ohno, H. *Phys. E* **2001**, *10*, 206.

(48) Wilson, M. J.; Xiang, G.; Sheu, B. L.; Schiffer, P.; Samarth, N.; May, S. J.; Bhattacharya, A. *Appl. Phys. Lett.* **2008**, *93*, 262502.